This work covers the effectiveness of the White tea extract as a green corrosion inhibitor and is correlated to the strength and stability bonding between the phenolic molecule and the Fe atoms in mild steel and how this interaction can be studied by altering the concentration and temperature. White tea has received considerable attention due to its capability as a corrosion inhibitor and has been extensively studied using electrochemical techniques. However, accurate and systematic functional group identification and surface modification have been missing. Our study sought to demonstrate the quantitative measurement of electrochemical impedance spectroscopy (EIS) complemented by the FTIR (Fourier transform infrared spectroscopy), Total Phenolic Test, and Raman Spectroscopy. The SEM (Scanning Electronic Microscope)/EDX (Energy-Dispersive X-Ray Spectroscopy), and AFM (Atomic Force Microscope) were used to study the surface modification. The EIS results show that the optimum inhibition efficiency was 96 % in a solution of 80 ppm at 60 °C. Acetone 70 % was used to extract White tea and gives 14.17±0.25 % phenolic compound. Spectroscopic studies show -OH, Aromatic C=C, C=O and C-O-C become major contributors in the adsorption process and are found on the surface of metals as corrosion protection. Meanwhile, the thermodynamic calculation shows the White tea was adsorbed chemically. The nearness of R^2 to 1 shows the adsorption agrees with the Langmuir adsorption isotherm. Eventually, the surface modification revealed that phenol molecules are responsible to reduce the corrosion rate at 16.38×10^{-3} mpy. Our results are expected to provide a guideline for future research in White tea as a green corrosion inhibitor

Keywords: catechin, green corrosion inhibitor, chemisorption, adsorption, surface modification, Langmuir isotherm

UDC 665
DOI: 10.15587/1729-4061.2021.224435

DEVELOPMENT OF WHITE TEA EXTRACT AS GREEN CORROSION INHIBITOR IN MILD STEEL UNDER 1 M HYDROCHLORIC ACID SOLUTION

Agus Paul Setiawan Kaban
Master of Engineering, Post-Graduate Researcher*
E-mail: rehrejeki@gmail.com
Aga Ridhova
Metallurgy and Materials Researcher***
E-mail: aga.ridhova@lipi.go.id
Gadang Priyotomo
Doctor of Engineering, Researcher
Research group of Materials Corrosion & Protection Technology***
E-mail: gadangp@gmail.com
Berna Elya
Professor of Pharmacy
Phytochemistry and Pharmacognition Laboratory
Universitas Indonesia
Gedung A Rumpun Ilmu Kesehatan Lantai 3, Kampus UI Depok, Jawa Barat, Depok, Indonesia, 16424
E-mail: berna.elya@farmasi.ui.ac.id
Ahmad Maksum
Doctor of Engineering
Department of Mechanical Engineering
Politeknik Negeri Jakarta
Jl. Professor Doktor G.A. Siwabessy, Kukusan, Kecamatan Beji, Depok, Indonesia, 16425
E-mail: ahmad.maksum@mesin.pnj.ac.id
Yunita Sadeli
Doctor of Engineering*
E-mail: yunce@metal.ui.ac.id
Sutopo
Professor of Engineering*
E-mail: sutopo@metal.ui.ac.id
Taufik Aditiyawarman
Master of Science
PT. Pertamina Hulu Energi
Jl. TB Simatupang No. Kav. 99, RT.1/RW.1, Kebagusan, Kec. Ps. Minggu, Kota Jakarta Selatan, Daerah Khusus Ibukota Jakarta, Indonesia, 12520
Department of Metallurgy and Material Engineering**
E-mail: taufik.aditiyawarman@pertamina.com
Rini Riastuti
Doctor of Engineering*
E-mail: riastuti@metal.ui.ac.id
Johny Wahyuadi Soedarsono
Doctor of Engineering, Professor
Department of Metallurgy and Material Engineering**
Email: jwsono@metal.ui.ac.id
*Department of Metallurgical and Materials Engineering
Center of Minerals Processing and Corrosion Research**
**Universitas Indonesia
Kampus Baru UI Depok, Jawa Barat, Indonesia, 16424
***Research Center for Metallurgy and Material
Indonesian Institute of Sciences
Kawasan Puspiptek Gd. 470, Serpong, Banten, Indonesia, 15314

Received date 08.02.2021
Accepted date 12.03.2021
Published date 12.04.2021

***How to Cite**: Kaban, A. P. S., Ridhova, A., Priyotomo, G., Elya, B., Maksum, A., Sadeli, Y., Sutopo, S., Aditiyawarman, T., Riastuti, R., Soedarsono, J. W. (2021). Development of white tea extract as green corrosion inhibitor in mild steel under 1 M hydrochloric acid solution. Eastern-European Journal of Enterprise Technologies, 2 (6 (110)), 6–20. doi: https://doi.org/10.15587/1729-4061.2021.224435*

1. Introduction

The purpose of this study is to determine the effect of the catechin molecule in White tea as a green corrosion inhibitor. This inhibitor impairs the corrosion in mild steel under acidic conditions. Commonly, this drawback occurred when metal is exposed to a low pH environment, acidic pickling, and acidification process and becomes one of the recurrent

challenges in oil wells. It also induces hydrogen embrittlement and fastens the rate of corrosion [1]. Although corrosion is a slow electrochemical process and occurs naturally, several protections, such as coating, cathodic protection, material selection, and introduction of the inhibitor demonstrate solutions to address the issue [2]. The presence of inhibitors has shown that inhibition is linked to adsorption processes. This strategy is frequently used and developed due to the cost-effectiveness at a given low volume of inhibitor solution [3, 4].

Recently, there has been renewed interest in harnessing the potential of the natural product (e.g. plants) as a green corrosion inhibitor. Several works have investigated the adsorption of plant extract exists in the formation of the passive film and how the interaction between the adsorbate and inhibitor influences the corrosion process in metal. For instance, the use of *Morinda citrifolia* reduces the effect of corrosive 3.5 % NaCl in low carbon steel [5], *Pluchea indica* depresses the electron activity at the anodic and cathodic sites [6], *Areca Flower* decreases the corrosion rate in low carbon steel through the interaction between polyphenolic/flavonoid compounds with steel [7], and Sweet Potato interrupts the oxidation process through the formation of chelating agent in complex compound Fe-anthocyanin [8] and Fe-ascorbic acids [9]. These examples of studies correlate to the ability of organic components to form chemical bonding with metal. Commonly, the high electronegativity atoms such as N, O, S, and P, and the presence of conjugation of π and σ bond are accountable for the strength of organic molecule (e. g phenol) adsorption on the metal [10].

It has previously been observed that the content of phenolic compounds in White tea is a key role to determine the effectiveness of the adsorption. However, the link between the total phenolic compound and the adsorbed functional groups on the surface of the mild steel has not been confirmed quantitatively and qualitatively. To address this issue and to fill this gap, we use the total phenolic content and state-of-art FTIR and Raman Spectroscopy to determine the type of bonding on the surface of metals. Moreover, to verify the result of adsorption, the utilization of SEM/EDX complemented by AFM has been made to confirm the adsorption process.

Therefore, studies that are devoted to this study are the explanation of the chemisorption process and how this chemical interaction correlates with the characterization results. It also unveils the formation of a dative covalent bond between the catechin molecules and 3d orbital of Fe ions based on the FTIR and Raman Spectroscopy data. Eventually, we will give a possible proposed inhibition mechanism according to various advanced surface characterization shreds of evidence that has been obtained thus far.

2. Literature review and problem statement

The papers [11, 12] present the result of the inorganic inhibitor in 50 μM clozapine and 2-methylimidazole. It is shown that clozapine has a high inhibition efficiency of 98 % while 2-methylimidazole reduces the corrosion current density to 1.9 mA cm^{-2}. These results can be associated with the ability of an inorganic inhibitor to modify the electrochemical reaction on the surface of metals. But there were unresolved issues related to the toxicity of the inorganic inhibitors. For instance, the improper utilization of clozapine may affect the number of white blood cells in the human body [13] while 2-methylimidazole affects human reproduction [14].

The result of the paper [15] acquires problems in preparing inorganic inhibitors, the cost to prepare the inhibitors, and the renewability of the raw materials. Owing to the presence of commercial 1,2,4-triazole (t) and imidazole, the major drawback may raise the manufacturing cost of inhibitors. Also, the operating temperature of the synthesized inhibition was only 40 °C. This shortcoming makes relevant research impractical.

Many researchers use plants to prepare inhibitors since plants are renewable materials and to prepare the extract requires inexpensive apparatus and chemicals with simple methodology. For instance, the results in [16] were used in preparing the extract of *Curcuma xanthorrhiza* at 1,000 ppm. The plant was extracted using 1M HCl with a single extraction method. The Electrochemical Impedance results analysis showed the inhibitor lowers the corrosion rate of the API 5L X42 steel in 1M HCl. Secang Heartwood (*caesalpinia sappan l*) extract was obtained using a mechanical process and dissolving the raw material in methanol [17]. The result shows the inhibitor achieved 53.18 % efficiency and behaves as a mixed-type inhibitor in a 3.5 % NaCl solution. Another extraction method shows that this plant can be extracted using isopropyl alcohol and water [18]. The inhibitor controls the charge transfer process at surface metal and electrolyte and gives high inhibition efficiency of 90 %. The anti-oxidant and tannin properties of plants can be also used as a potential candidate for green corrosion inhibitors. Recent work from [19] shows the presence of *manikara zapota; garcinia mangostana l., and ipomea batatas* can effectively reduce the corrosion rate on the API 5L steel by the adsorption process of their functional groups on the surface of the substrate. This research finding was confirmed by [20] showing that the heteroatoms of oxygen in Epigallocatechin Gallate (EGCG), which contains a phenolic compound and hydroxychavicol, are accountable for the formation of the passive layer.

Despite several studies on White tea as an inhibitor are available, only a few researchers considered the challenges of their preparation when used at low concentrations. In this study, we present a single step to extract White tea that gives a high content of phenolic compound with slight modifications. Herein, we use acetone with high concentration and longer infusion time. The reason for this is correlated with the ability of phenolic compounds in White tea to dissolve in a polar solvent. Without extraction modification, the inhibitor would only exhibit low heteroatom reactivity [21] and low adsorption coverage [22].

White tea contains a catechin molecule that exhibits a sufficient amount of oxygen and delocalized π-electrons (Fig. 1).

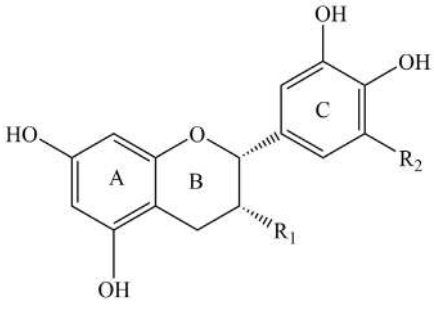

Fig. 1. Catechin molecule

The molecule has four different derivative molecules such as Epicathechin (EC), Epicatechin-3-Gallate (ECg), Epigallocathechin (EGC), and Epigallcatechin-3-Gallate (EGCg) as reported previously [23].

Hence, these molecules are predicted to be adsorbed on the surface of metal shown by its functional group as reported by the other work [24]. However, as previously published [25], the accurate determination of specific functional groups attached to the surface of the metal was not clearly explained. To overcome this difficulty, in this present work, we utilized the FTIR complemented by Raman Spectroscopy as a powerful technique to achieve this objective. Similarly, the research [15] has used Raman Spectroscopy to reaffirm the functional groups on the protective film on the metal.

To study the performance of the adsorbed inhibitor and activation processes, the effect of temperature is discussed. It correlates to the thermodynamic calculation of ΔH_{ads}, ΔG_{ads}, and ΔS_{ads}. The study [21] shows that organic inhibitors are not suitable to protect the metal from corrosion due to instability and insolubility at higher temperatures. A sufficient extracted phenolic compound adsorbed chemically on the surface of metal would address this shortcoming. The reason for this may be correlated to the presence of multiple electron-donating -OH groups in the phenolic group. It intensifies the interaction between the catechin molecule and the metallic surface by increasing the number of adsorption sites on the inhibited surface [26]. A similar approach was used in [27] however, it is predicted that the catechin molecule would have a higher surface coverage area (θ) with the greater thermal stability of inhibition due to its planarity and molecular size.

The calculation value of R^2 on the Adsorption Isotherm model is used to verify the nature of the inhibitor on the metal surface. The slope of the calculated graph describes the number of active sites on the inhibited surface. The calculation suggests that the value of the thermodynamics parameter would prove the stability of the inhibitor at elevated temperature.

The effects of adsorption correlate to the surface modification by the inhibitor. The paper [28] has explained that SEM is suitable to characterize the surface of inhibited steel in an acidic medium. However, the roughness of the inhibited surface was not calculated quantitatively and described comprehensively. This information is necessary to explain the hydrophobic nature of the inhibitor and to support the evidence given in SEM/EDX characterization. In this work, we combine the SEM/EDX method with AFM results to provide important support towards the chemical and electrochemical reactions between the inhibitor and the metals.

3. The aim and objectives of the study

The aim of this study is to present for the first time a quantitative and qualitative analysis of *WT.E* as natural corrosion inhibitor for mild steel. The discussion covers the aspect of electrochemical, functional groups, extraction methods, thermodynamics and surface analysis.

To achieve these aims, the following objectives are accomplished:

– characterization of White tea extract to study the reduction of corrosion rate using EIS;

– determination of total phenolic content of the White tea extract;

– characterization of functional groups to study the types of functional adsorbed on the surface of the mild steel using FTIR and Raman spectroscopy;

– determination of thermodynamics inhibition parameters and mode of adsorption;

– characterization of the surface of the mild steel to prove the process adsorption using SEM/EDX and AFM.

4. Materials and methods

4. 1. Preparation of inhibitor solution

The inhibitor solution was prepared using the extraction method [29] with a slight improvement in terms of temperature and duration of extraction. Extraction of phenol was conducted using 15 ml acetone 70 % for one gram of the ground White tea leaves. The solution was heated using a Soxhlet extractor inside the water bath at 70 °C within 1 h to ensure the heat was uniformly distributed. The inhibitor 20, 40, and 80 ppm solutions were prepared by dissolving the required amount of inhibitor in 1M HCl. The dilution of HCl 37 % solution (Merck.Co) was used to prepare HCl 1M solution using distilled water.

4. 2. Preparation of the working electrode and anti-corrosion EIS measurement

The working electrode used in this experiment was categorized as mild steel. The main elemental composition of the electrode is presented in Table 1.

Table 1

Elemental composition of the working electrode

Element	Fe	C	Mn	Cr	Cu	Zn	Sn	Mo	W
Percentage	98.34	0.32	0.52	0.22	0.2	0.053	0.021	0.009	0.007

The methods of preparing the working electrode and EIS measurement were done based on our previous unpublished work. The chemical composition of the mild steel coupons (wt %) of C (0.32), Si (0.19), S (0.01), P (0.006), Mn (0.52), Ni (0.05), Cr (0.22), Mo (0.009), V (0.006), Cu (0.2), W (0.007), Ti (0.003), Sn (0.021), Al (0.007), Pb (0.017), Nb (0.007), Zr (0.007), Zn (0.053), Fe (98.34) was provided by the Karakatau Steel. Co. The rod specimen was cut cross-sectionally with a thickness of 1 cm, connected to Cu wire, and mounted to achieve an exposed surface area of 3.14 cm^2. The grinding process was carried out to remove the oxide layer on the specimen using the SiC paper until grit #600 (refer to ASTM G 59 standard) was achieved. Further, the specimen was washed with water and dried. The entire electrochemical measurements were carried out using the Gamry Instrument of G750 series connected and controlled by an electrochemical analyzer. The mounted mild steel acts as a working electrode; the auxiliary electrode was Pt (the surface area 1 cm^2) and the reference saturated calomel Ag/AgCl electrode (SCE). The potential measurements were provided versus the SCE electrode. The Tafel Polarisation measurement at OCP spans from -200 and to +200 mV. The applied scan rate was 1.5 mV/s. The Tafel cathodic, and anodic slopes (β_c and β_a), corrosion potential (E_{corr}) and corrosion current density (i_{corr}) were obtained upon the

completion of Tafel Curve Fitting. A typical calculation for inhibition efficiency was given in equation (1),

$$\left\{\%\eta = \frac{R_{corr} - R_{inh}}{R_{corr}} \times 100\,\%\right\}, \quad (1)$$

where R_{corr} and R_{inh} are the corrosion and the film inhibitor resistance ($\Omega\,cm^2$). This methodology is modeled by the Gasometric method where the corrosion reaction is defined by the amount of the deliberated hydrogen gas, which is proportional to the rate of corrosion [30].

4. 3. Total phenolic measurements

The major component of phenol was determined by the Folin-Ciocalteu reagent [31] using gallate acids as the standard solution. To 4 ml of distilled water, 250 μL of Folin-Ciocalteu reagent followed by mixing 25, 50, 100, 150, and 200 μL were added and stirred. After 8 min, 750 μl of 20 % Na_2CO_3 was added and stirred homogeneously. Subsequently, the mixture was left for 2 h at room temperature. The Gallic Acid Equivalents (μg/mL) were expressed because of absorbance measurements at 760 nm. The measurement was done twice and the result was given by the linear regression method.

4. 4. Functional groups and surface analysis studies

The functional group characterization of *WT.E* extract before and after the formation of the film was performed using FTIR (Shimadzu). Moreover, the interaction between the phenol molecules in *WT.E* extract and Fe-atom after immersion at 60 °C was studied using Raman spectroscopy (Horiba iHR (1,024×256-OE) with CCD Detector (Wright 1,024×256 pixels). Similar to Calderon [32], the untreated mild steel Raman spectra were used as a comparison. Before characterization, the mild steel was rinsed with distilled water and kept in the free-air desiccator to avoid the formation of an oxide layer. The SEM micrograph was used to study the surface morphology (JEOL Type JSM 6390) and complemented by EDX analysis to determine the chemical composition of Fe, O, and Cl after the substrate was exposed in 1M HCl.

The characterization of the surface degradation is provided by three-dimensional AFM (NX10 Atomic Force Microscopy, Park System) as an accurate prediction tool to study the adsorbed passive film.

5. Results of the catechin molecules in White tea

5. 1. Results of spectroscopy measurement of White tea inhibitor

5. 1. 1. Electrochemical impedance spectroscopy

Table 2 shows the EIS measurement of the inhibitor at different concentrations and temperatures. From Table 2, the smaller relativistic values of R_{inh} and $C_{dl\text{-}inh}$ have been carefully observed as the effect of increasing temperature for all inhibitor concentrations. This fact correlates with the intrinsic behavior of protected film and surface inhomogeneity [33], the mobility of the ions [6], and the thickness of the total protected film porosity [15]. Equations (1) and (2) are used to determine the inhibition efficiency (%η) and capacitance double layer, C_{dl} [16],

$$\left\{C_{dl} = \left[Y_0 \times \left\{\exp\left[1/n\right]\right\}\right] \times \exp\left[\frac{1-n}{n}\right] \times \left(\frac{R_s R_{ct}}{R_s + R_{ct}}\right)\right\}, \quad (2)$$

R_{ct} and R_{inh} are the charge transfer and the film inhibitor resistance ($\Omega\,cm^2$). Y_0 and n are the passivity $\left(\times 10^{-6}\ \Omega^{-1}cm^{-2}S^n\right)$ and layer thickness, respectively.

Table 2

Electrochemical impedance parameters of mild steel in 1M HCl with inhibitor

C (ppm)	Temp (°C)	R_{inh} ($\Omega\,cm^2$)	R_{ct} ($\Omega\,cm^2$)	CPE		Corrosion Rate, (mpy) $\times 10^{-3}$
				Y_0 $\left(\times 10^{-6}\ \Omega^{-1}cm^{-2}S^n\right)$	n	
Blank	25	10.35±0.23	0.38±0.23	2.23	0.864	4.377
Blank	50	1.28±0.06	0.20±0.06	2.17	0.924	40.34
Blank	60	0.2±0.07	0.40±0.07	19	0.777	122.2
20	25	14.55±3.42	8.14±3.72	4.11	0.739	3.491
20	50	2.89±0.29	0.47±0.28	2.66	0.809	29.44
20	60	1.22±0.11	0.43±0.10	4.53	0.818	61.39
40	25	22.62±1.29	0.88±1.09	3.41	0.725	3.08
40	50	4.60±0.26	0.63±0.24	2.30	0.796	19.95
40	60	2.33±0.18	0.46±0.17	1.80	0.828	38.29
80	25	16.06±0.30	0.32±0.06	0.64	0.917	3.027
80	50	4.37±0.14	0.42±0.13	4.33	0.741	11.59
80	60	5.90±0.62	1.05±0.58	1.21	0.8	16.38

Another parameter of ideal capacitance of double layer is C_{dl}. This parameter was generated from the EIS results and used to indicate the thickness of the passive film in terms of replacement of water molecules with White tea inhibitor molecules at the metal/electrolyte interface.

Table 3 compares the capacitance double layer of inhibitor, $C_{dl\text{-}inh}$ and the capacitance double layer of bulk solution, $C_{dl\text{-}bulk}$. These values indicate the thickness of inhibitor film and roughness of the metal surface [34]. It can be derived from the table, $C_{dl\text{-}inh}$ is higher than $C_{dl\text{-}bulk}$ in an inhibitor solution of 80 ppm at any temperatures. This is evidence that the inhibitor covers the pit corrosions and increases the heterogeneity of the surface of the treated mild steel.

Table 3

Comparison of capacitive double layer of bulk and inhibitor

Concentration (ppm)	Temperature (°C)	$C_{dl\text{-}bulk}$	$C_{dl\text{-}inh}$	η (%)
Blank	25	1.99	0.02	0
Blank	50	1.97	9.43	0
Blank	60	29.20	20.25	0
20	25	6.06	0.54	28.87
20	50	2.47	8.02	55.72
20	60	4.51	6.78	81.03
40	25	3.75	3.62	54.24
40	50	2.07	8.26	72.17
40	60	1.52	5.55	90.03
80	25	0.53	10.92	35.55
80	50	4.22	6.95	70.77
80	60	0.99	6.43	96.06

In addition, the Nyquist plot (Fig. 2) obviously demonstrates the variation in anti-corrosion performance among the solutions before and after the addition of inhibitor. The worst protection was given by the incompleteness semi-circle of the Nyquist plot at 25 °C (Fig. 2, *a*). Whilst, the similar magnitude of low-frequency impedance at 20 and 40 ppm in Fig. 2, *b* shows an improvement of anticorrosive film of inhibitor. At 60 °C, the addition of inhibitor shows less penetration of chloride ions and water molecules due to the presence of a passive protective layer of White tea inhibitor. This performance correlates to the completeness diameter of the capacitive loop with the increase in White tea inhibitor concentration and maximum impedance was given at 7.5 Ω cm^2.

The most interesting aspect of this graph in Fig. 2, *c* is the evaluation of corrosion resistance of the inhibitor. The most striking result to emerge from this measurement is the consistency completeness semi-circle capacitive loops with the Nyquist plot at 60 °C. This phenomenon was attributed to the ability of inhibitor to minimize the volume of protection (220 ml/cm^2) per surface area as a protection and to provide a layer so that the effect of attacked aggressive ions can be reduced.

As expected, the EIS results of the Nyquist and Bode plots are well fitted in Electrical Equivalent Diagram. This model represents the CPE bulk and CPE inh, which indicates corrosion protection by the presence of passive film. The Equivalent diagram of one-time and two-time constant diagram is shown in Fig. 3, *a*, *b*. *Rs*, R_{ct} and R_{inh} are the solution resistance, the charge transfer resistance, and the resistance of inhibitor, respectively. C1 CPE is the Constant Phase Element bulk solution that models the behavior of double layer (imperfect capacitor). CPE-inh is the double layer behavior of film inhibitor.

The results of inhibition efficiency, %η, are presented in Table 3. From the study table, the decrease of $C_{dl\text{-}Inh}$ and $C_{dl\text{-}bulk}$ corresponds to the increased value of protective coating thickness or lower dielectric constant [14] as more water molecules are displaced by the inhibitor at the metal/electrolyte interface [15]. So, the optimum protection, %η, of 97 % was given in the 80 ppm solution at 60 °C (Fig. 3, *b*).

As shown in this work, the Bode and the Nyquist plots are fitted well in Electrical Equivalent Diagram (Fig. 3, *a*) and used to elaborate the physical corrosion control at different concentrations of *WT.E* at 25 °C (Solution A) and 60 °C (Solution B). The initial and final low-frequency impedance at solution A was 1.0373 and 1.1404 Ω cm^2, respectively. Moreover, the Nyquist plot clearly shows the appearance of one semi-circle for solution A. Although, the low-frequency impedance in the Bode plot of solution B increases from 0.07628 Ω cm^2 to 0.86652 Ω cm^2, the overall impedance has decreased as a more concentrated inhibitor was added. This result well agrees with the presence of one complete semicircle in the Nyquist plot at the same condition (Fig. 2, *b*).

The twin-wide shoulder of the Bode Phase in Fig. 4, *b* shows a perfect match with one capacitive loop in the Nyquist plot and resulting from the thickness of the adsorbed passive film increases. The resistance inhibitor R_{inh} and the capacitance double layer, Cdl_{inh}, are also worth clarifying the impedance behavior.

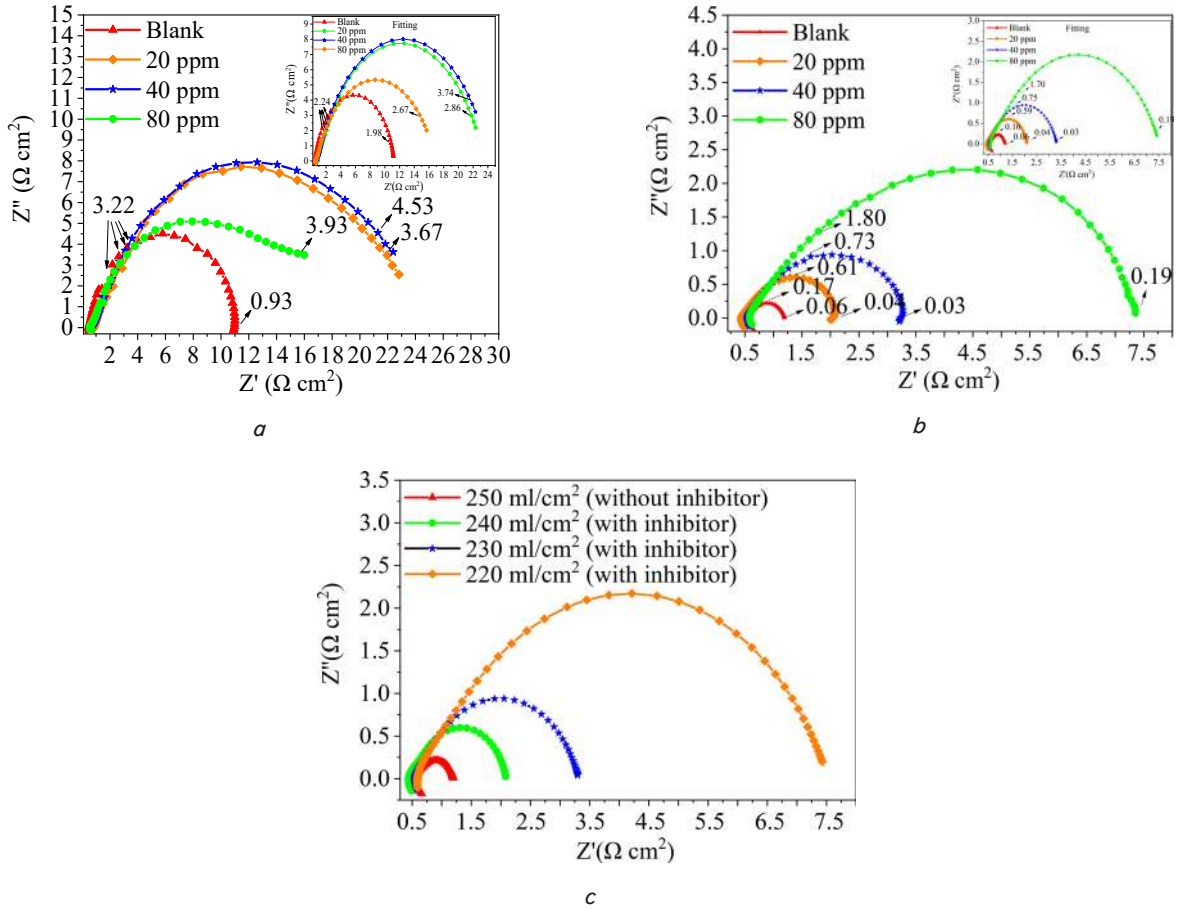

Fig. 2. Nyquist plot: *a* — various concentrations at 25 °C; *b* — various concentrations at 60 °C; *c* — volume/area of inhibition of the mild steel

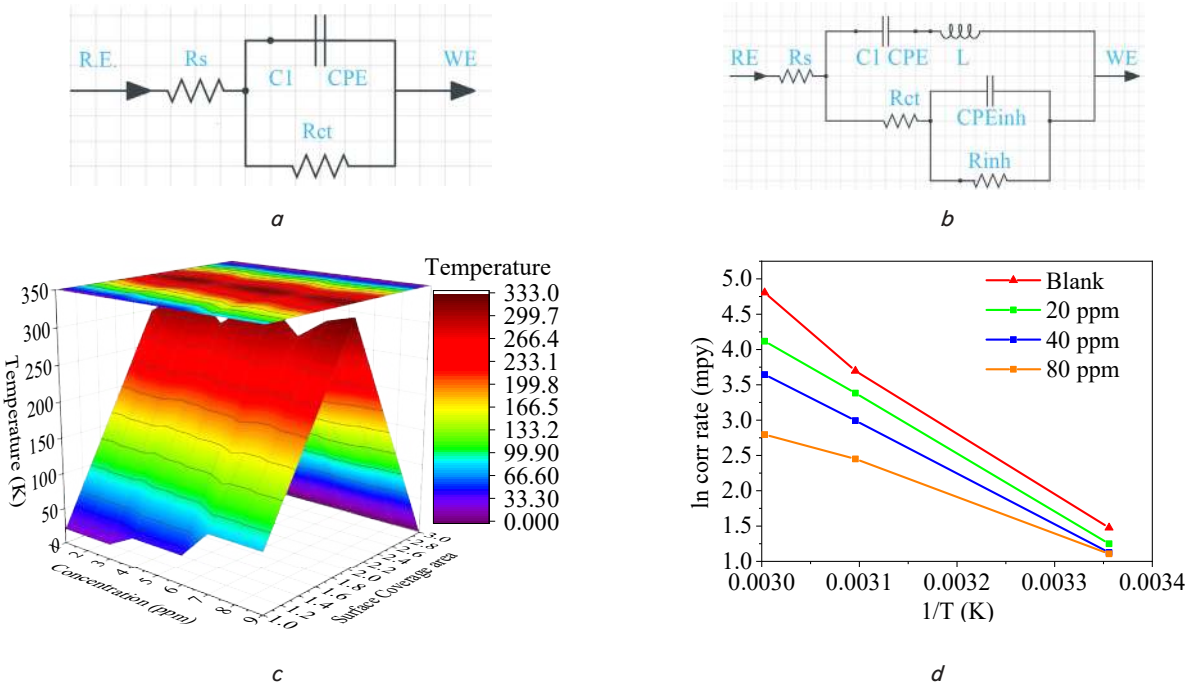

Fig. 3. Inhibitor effect in terms of: *a* — electrical equivalent circuit of white tea inhibitor one-time constant; *b* — electrical equivalent circuit of white tea inhibitor two-time constant; *c* — schematic 3D-surface coverage area of inhibition; *d* — corrosion rate of the mild steel with temperature variations

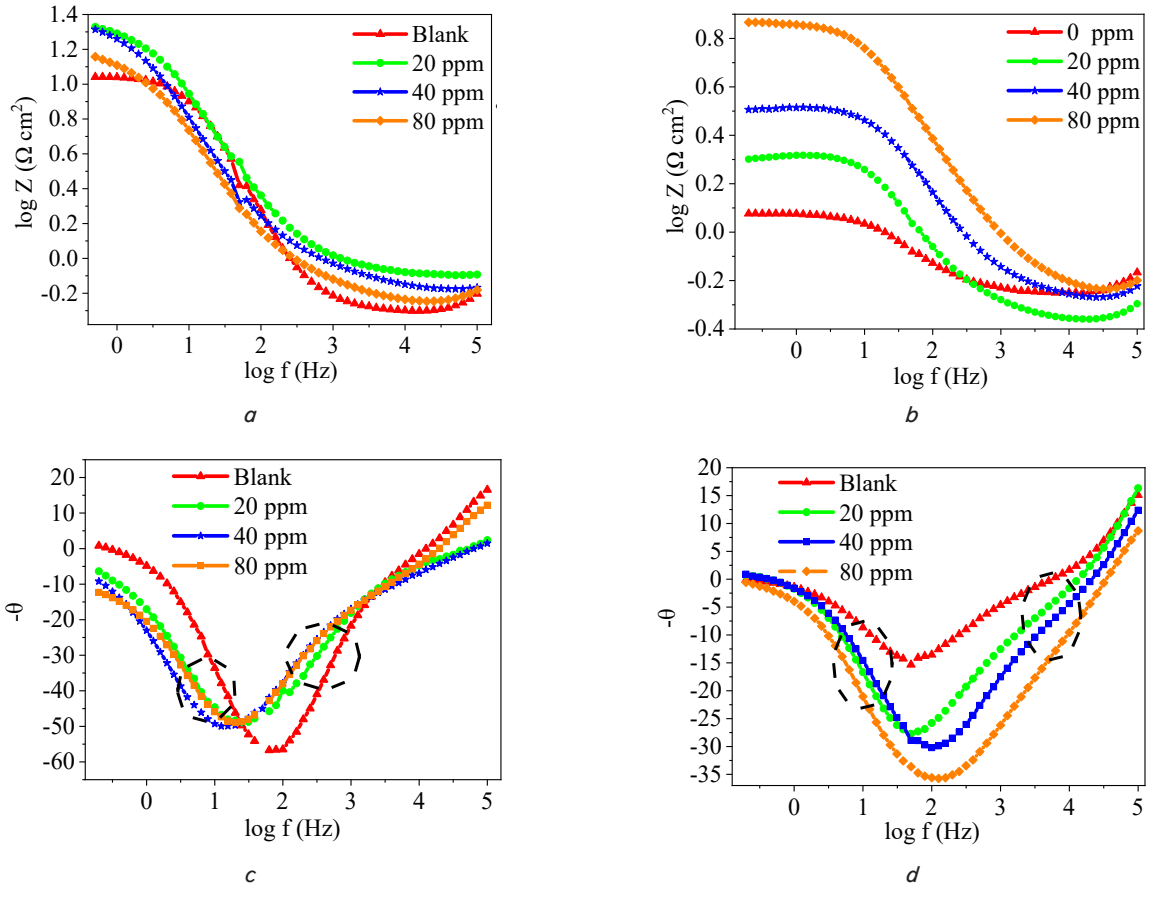

Fig. 4. EIS results in terms of: *a* — Bode Modules at 25 °C; *b* — Bode Modules at 60 °C; *c* — Bode Phase at 25 °C; *d* — Bode Phase at 25 °C

5. 1. 2. FTIR and Raman spectroscopy

Fig. 5, *a* shows the FTIR spectrum of the pure solution of 80 ppm and the inhibited solution. This study confirmed the presence of the functional groups both on the inhibitor and on the film of WT.E. The contribution of the spectroscopy technique to confirm the type of bonding between the adsorbate and the substrate surface is promising [34]. As can be seen, the presence of the functional group of -OH, Phenyl, C=O, Aryl C=C, CH_2, and C-O dominates both on the spectrum. The spectrum of FTIR is in good agreement with the results in the Raman spectroscopy and is presented in Fig. 5.

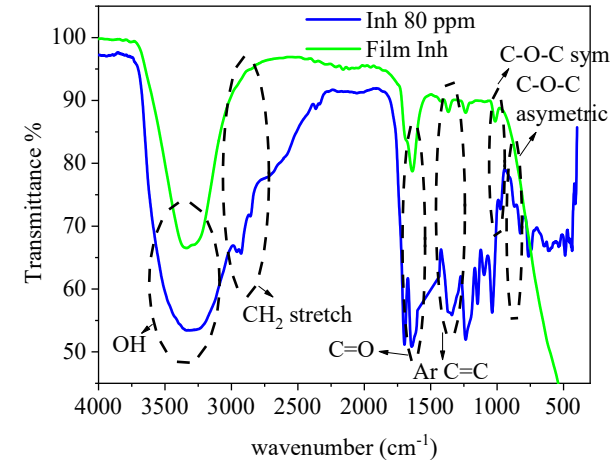

a

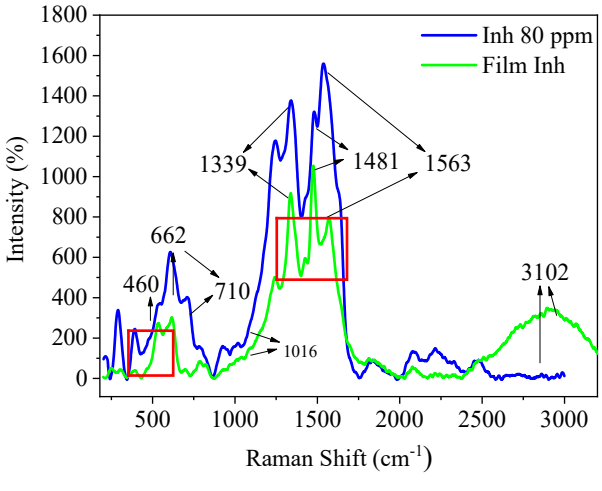

b

Fig. 5. Spectroscopy spectrum of the inhibitor in the absence and presence of inhibitor: *a* – FTIR; *b* – Raman

Fig. 5, *b* shows the Raman spectra of the inhibited mild steel in *WT.E* 80 ppm at 60 °C and the uninhibited steel at 25 °C as a comparison. The peaks are mainly located at the same level and trend with different intensity. The selected range of Raman shift is 400 3,200 cm^{-1} and is used to clarify the adsorption process of the specific functional group on the surface of the metal. This spectrum provides evidence that several active functional groups such as -OH, Aryl C=C, C=O, C-O-C are adsorbed on the metal. It also can be seen that the peak pattern of the *WT.E* film is aligned with the inhibitor solution of 80 ppm at 25 °C. This consistency shows the intense enhancement from the Raman spectrum to characterize the inhibitor performance on metallic surfaces.

5. 2. Total phenolic content in White tea

Table 3 summarizes the absorbance of various concentrations of 80 ppm White tea extract. The higher absorbance was given by the increasing concentration at 40 µg/ml. The total phenol content (TPC) was determined spectrophotometrically in the presence of Folin-Ciocalteu's reagent. The best linear fitting of concentration versus absorbance gave y=0.0969x–0.1032 with R^2=0.9977 (Fig. 6). The TPC was calculated using equation (3) [35]

$$\{TPC(\%) = C_1 \times V / m\}, \quad (3)$$

C_1 is the concentration of gallic acid from the calibration curve (mg/ml), m is the weight of the plant extract (g) and V is the volume of the extract (ml). Moreover, the TPC was quantified as gallic acid equivalents (GAE).

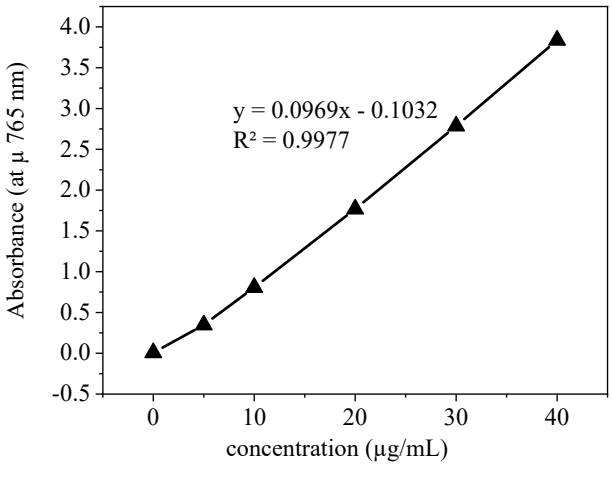

Fig. 6. Linear fitting concentration curve

The result of the total phenolic content is shown Table 4.

Table 4

Atomic absorption spectroscopy spectrum of total phenolic content

Concentration (µg/ml)	Absorbance		
	*A*1	*A*2	*A* (average)
0	0.0075	0.0059	0.0067
5	0.3036	0.3929	0.3483
10	0.7734	0.8415	0.8075
20	1.6721	1.8640	1.7681
30	2.7047	2.8663	2.7855
40	3.6624	4.0114	3.8369

The determination of total phenolic content gives clear guidance to the amounts of phenolic compounds in the White tea. In agreement with another researcher [36], the concentration of gallic acid correlates to the absorbance of the molecule as shown in Table 4. This value suggests that the phenolic content enhances the antioxidant properties of the White tea and increases the possibility for the White tea to adsorb in the form of passive film.

5. 3. Thermodynamics of the electrochemical process

Table 5 gives the thermodynamics results of the electrochemical process at various temperatures and concentrations. The 80 ppm solution at 60 °C shows superior protection as it has the highest surface coverage area (0.961).

Table 5

Thermodynamics parameter, surface coverage and K_{ads} calculated result

C (ppm)	Temp (K)	Surface Coverage (θ)	K_{ads} (L mol^{-1})	ΔG_{ads} (kJ/mol)	ΔH_{ads} (kJ/mol)	ΔS_{ads} (kJ/mol)
20	298	0.289	0.020	-24.572	15.295	133.782
20	323	0.557	0.063	-29.672	16.578	143.190
20	333	0.810	0.214	-33.975	17.091	153.352
40	298	0.542	0.030	-25.511	12.797	128.551
40	323	0.722	0.065	-29.753	13.871	135.058
40	333	0.900	0.226	-34.130	14.300	145.436
80	298	0.356	0.007	-21.899	23.916	153.741
80	323	0.708	0.030	-27.707	25.923	166.037
80	333	0.961	0.305	-34.962	26.725	185.246

The effectiveness of inhibition depends on the adsorption stability of the *WT.E* extract. The stability of the film correlates with equilibrium adsorption and desorption constant (K_{ads}) and the standard free energy of adsorption (ΔG_{ads}), entalphy change adsorption, ΔH_{ads}, and the entropy of adsorption, ΔS_{ads}. The unit of ΔH_{ads}, ΔG_{ads}, and ΔS_{ads} are in kJ/mol. The value of R is 8.314 J/K mole and T is the absolute temperature in K.

Equation (4) shows the relationship between ΔG_{ads} and K_{ads},

$$\left\{\Delta G_{ads} = -RT\ln\left(1\times10^{6}K_{ads}\right)\right\}. \quad (4)$$

Clarifying the calculated result of K_{ads}, the maximum value of K_{ads} is 0.305 and this value inverses with the [*WT.E*] at different temperatures. Moreover, it indicates the greater adsorbed inhibitors on the metal surface when the temperature of the system is beyond 50 °C. Accordingly, the range of ΔG_{ads} is –24.5 kJ/mol and –34.9 kJ/mol. Therefore, we conclude that the inhibitor is chemisorption at higher temperature. The negative value of ΔG_{ads} confirms the feasibility of adsorption and the stability of the passive film. Equation (5) is used to determine the value of ΔH_{ads} [37],

$$\left\{\ln K_{ads} = -\frac{\Delta H_{ads}}{RT} + k_2\right\}. \quad (5)$$

The plotting of ln K_{ads} vs T^{1} (5) is used to predict the heat of adsorption, ΔH_{ads} and to describe the coverage protection as the function of temperature. While the calculated entropy is given in (6).

$$\left\{\Delta S_{ads} = \frac{\Delta H_{ads} - \Delta G_{ads}}{\Delta T}\right\}. \quad (6)$$

The maximum value of ΔH_{ads}, 26 kJ/mol, ensures the spontaneity of adsorption. According to the literature, the range of ΔH_{ads} within 5–10 kJ mol^{-1} and 30–70 kJ mol^{-1} is referred to physisorption and chemisorption, respectively [38]. Our findings show that the range of ΔH_{ads} is 15–26 kJ mol^{-1}. This value supports the value of ΔG_{ads} and shows that the inhibitor preferably acts as chemisorption. It is clear from Table 5, the value of ΔS_{ads} indicates that the solid-liquid interface increases upon the adsorption process. The positive value of ΔS_{ads} elicits that the thermal stability of the film increases at elevated temperature and their irreversibility process [6].

Moreover, the (corrosion inhibitor) CRinh, A, R, and T are components of the corrosion rate (mpy), Arrhenius pre-exponential factor, activation energy upon addition of inhibitor (kJ mol^{-1}), absolute temperature (K) and universal gas constant. The slope of the linear plotting versus T^{1} determines the value of activation energy.

$$\left\{\ln CR_{inh} = \ln A - \frac{E_a}{RT}\right\}. \quad (7)$$

The calculated result of activation energy is shown in Table 6. It shows in the absence and presence of the inhibitor, E_a was 76.88 and 40.49 kJ mol^{-1}. The presence of inhibitor at any concentration decreases the value of activation energy.

Table 6

Activation energy of the mild steel immersed in white tea inhibitor extract

Inhibitor	Inhibitor concentration (ppm)	E_a (kJ/mol)	R^2
Without inhibitor	0.0	76.88	0.9943
White tea inhibitor	20	67.73	0.999
	40	59.49	1
	80	40.49	0.9962

The presence of *WT.E* was seen to lower the value of E_a, suggesting that the inhibitor is more effective at higher concentrations and reverses the physisorption mechanism [39]. The interaction between the inhibitor particles and the surface proves the chemical bonding has occurred and decreases the value of E_a nearly 70 %.

5. 4. Adsorption isotherm of inhibition

The classification of the type of adsorption and adsorption isotherm of inhibition is useful. This information estimates the effect of corrosion temperature on the interaction between the inhibitor molecules and substrate on the metal surface [40].

Table 6 shows the calculated R^2 to determine the adsorption inhibition model. The plotting between C/θ against $1/K_{ads}$ in Equation (8) gives the value of R^2

$$\left\{\frac{C}{\theta} = \frac{1}{K_{ads}} + C\right\}, \quad (8)$$

where the variables θ, K_{ads}, and C are the surface coverage area fraction, adsorption/desorption constant (mol·L^{-1}), and the concentration of *WT.E* inhibitor (mol·dm^{-3}). The calculation of θ is derived from the electrochemical measurements at different temperatures and concentrations.

Most calculations of R^2 are close to 1 and indicate the interaction of inhibitor with the surface forms a mono-layer passive film by restricting the intermolecular and intramolecular forces [41]. The value of R^2 closer to 1 confirms the Langmuir adsorption isotherm model and provides experimental interaction between the inhibitor and surface of the metals [42].

5. 5. Surface studies

5. 5. 1. Scanning electronic microscope and EDX

Fig. 7, *a*, *b* shows the SEM of the mild steel in the absence and presence of the inhibitor complemented by the measurement of elemental composition (EDX) in various concentrations.

Without protection, mild steel experiences severe corrosion and cracks (Fig. 7, *a*). This is the result of the dissolution of the corrosive solution of HCl 1M. In contrast, the protected surface of the metal is shown by the presence of the adsorbed film and covers the pitting corrosion and cracks (Fig. 7, *b*). The EDX results show that the presence of Fe, O, and Cl is presiding in each EDX measurement. Moreover, the addition of inhibitor increases the elemental percentage of oxygen as a result of adsorption of phenolic compounds.

5. 5. 2. Atomic force microscope (AFM)

The 3D AFM images of the mild steel before and after exposure in *WT.E* solution for 24 h are presented in Fig. 8.

This image explains the surface modification by the adsorbed film and the quantitative calculation on the AFM data. The 3D-AFM image of treated steel shows that the presence of the inhibitor has modified the surface of the metal and increases the hydrophobic nature of the passive film. The quantitative calculation of the film roughness and the skewness parameter was done using an open-source of Gwyddion. The root-mean-square roughness of the uninhibited and inhibited mild steel was 774 nm and 585.1 nm, respectively. According to the author [43], the calculation of the skewness parameter can be obtained using eq. (9).

$$\left\{S_{sk}=\frac{1}{M\times N\times RMS^3\left[\sum_{j=1}^{N}\sum_{l=1}^{M}\eta\left(X_lY_j\right)^3\right]}\right\}, \quad (9)$$

where:

– M – number of points per profile;

– N – number of profiles;

– RMS – root mean square of the sampling area;

– $\eta(x, y)$ – rough surface data set.

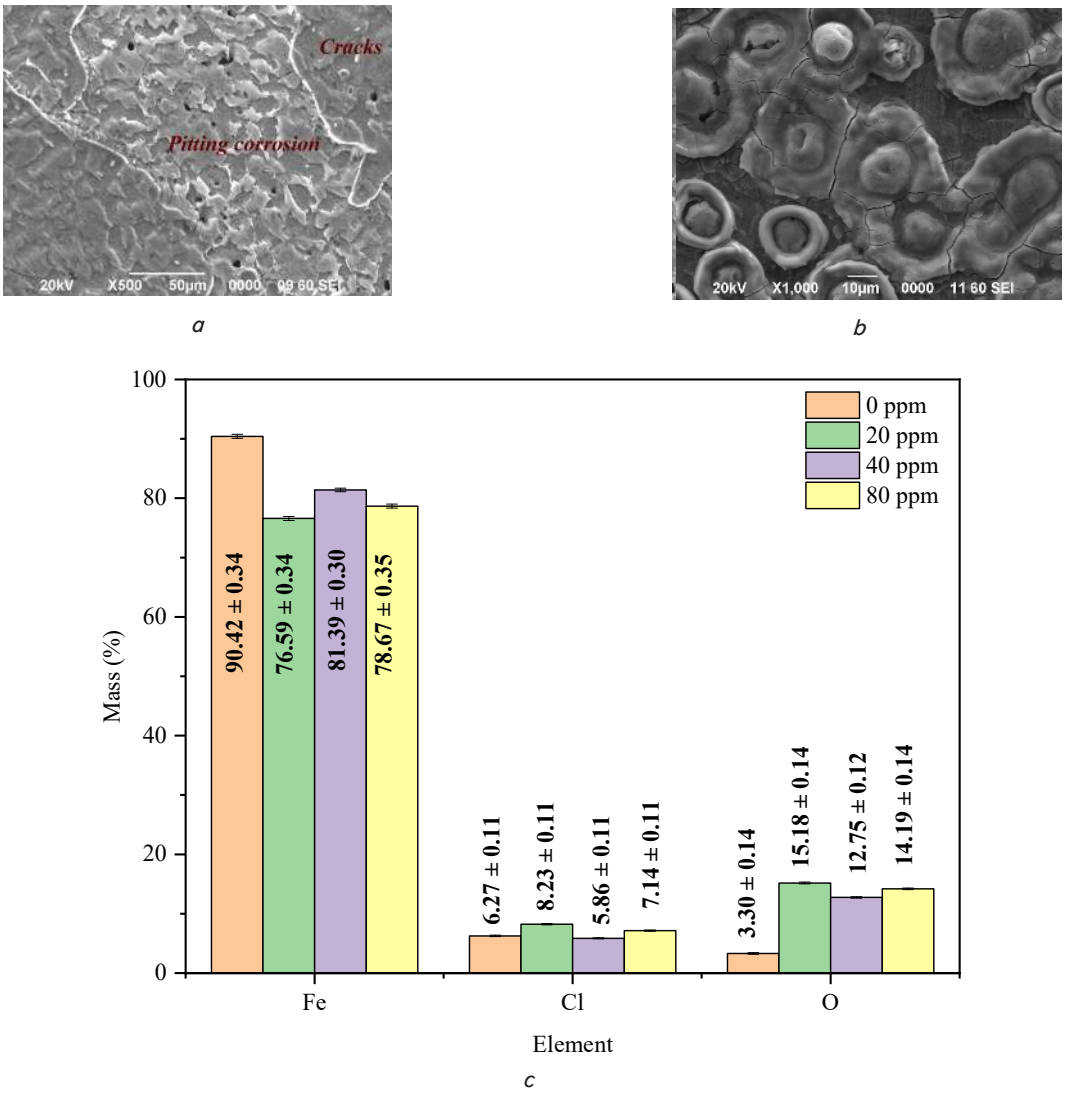

Fig. 7. SEM images of: *a* — uninhibited; *b* — inhibited mild steel; *c* — EDX histogram of varied concentration

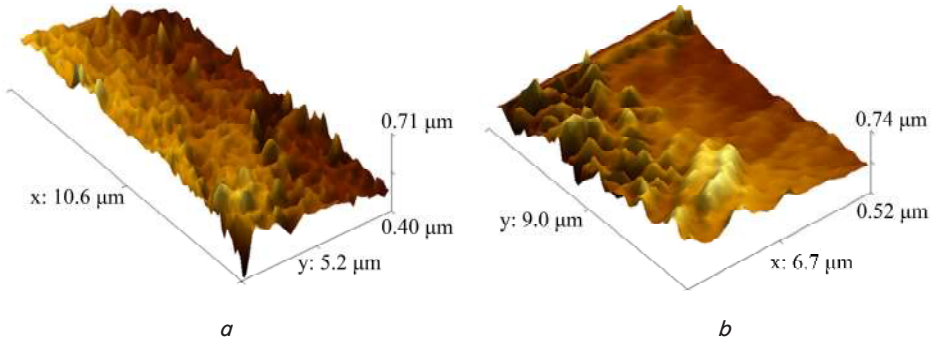

a *b*

Fig. 8. 3-D AFM images of: *a* — untreated; *b* — treated mild steel 80 ppm inhibitor

We report that the SSK for the non-inhibited and inhibited surface is 0.2714 and 0.4744 and these values are comparable to Noorbakhsh [44].

6. Discussion of the results of the effect of White tea inhibitor addition on the surface of mild steel

Characterization of White tea extract using spectroscopic methods, the effect of phenolic compound, the discussion on the FTIR and Raman spectra, the effect of temperature on the thermodynamics of inhibition and the film adsorption process on the surface are discussed in this section. Also, the economic value in inhibitor manufacturing is intensively elaborated.

In this present research, we use EIS as an experimental approach to describe the interaction between the inhibitor and the working electrode at different concentrations and temperatures. The main feature of EIS due to this method is a continuous, fast, reliable and reproducible technique as stated in the previous research [45]. Fig. 4, *a*, *b* shows two shoulders of two time constants shown in the Bode plots despite only a single depressed capacitive loop is visible in the Nyquist plot (Fig. 2, *b*). The wide shoulder in Fig.4, *a* at higher frequency can be associated with the dielectric properties, which behaves like a charged capacitor, CPE 1, and limiting electrochemical reaction. The optimum protection and passivation of inhibitor were shown by the combination between the small shoulder (Fig. 4, *b*) at lower frequencies and a depressed capacitive loop (Fig. 2, *b*). For all concentrations of inhibitor at 60 °C, the value of R_{inh} is greater than R_{ct} which makes the value of Capacitance double layer inhibitor, Cdl_{inh} significantly higher than Capacitance double layer, $Cdl_{\text{-}bulk}$.

This fact explains the completeness of depressed capacitive loop in the Nyquist plot (Fig. 2, *b*). Also, the optimum protection of the inhibitor was given by the larger value of R_{inh} (5.90±0.62 Ω cm^2) compared to R_{ct} (1.05±0.58) at 80 ppm and 60 °C. This pronounced discrepancy provides the benefit of increasing concentration and temperature on the inhibited over the uninhibited mild steel decreases the corrosion rate at 16.38×10^{-3} mpy. A comparable finding is supported and given by Gomelya [30].

This value elicits that the chemical impermeable structure of the benzene ring and the presence of phenol groups in the molecule of catechin become a major contributor in the adsorption process of the passive film. The adsorption of passive film can be identified by taking a closer observation on the calculated value of *n*, surface inhomogeneity. Based on Table 2, the value of *n* increases from approximately 0.7 to 0.8 at 20 and 40 ppm inhibitor solution but slightly decreases at 80 ppm. This fact also explains that the addition of inhibitor solution of any concentration increases non-homogeneities surface as a result of thicker mono-layer film formed.

As outlined previously, in solution A, the formation of the unresolved impedance graph is seen (Fig. 4, *a*). A comparative study to verify this observation is to investigate the semi-circular loop at 60 °C. The results of [6] argued that at a temperature above 60 °C, the movement of the species is significant. The correction of this single assumption is addressed by explaining the effect of the thermal strain. The passive film experiences stress at various temperatures. Stress produces a strain that occurs either in the same plane or in the perpendicular direction of the film [21]. In contrast, all impedance spectra give a single semicircle loop in solution B (Fig. 2, *b*). This one-time constant graph features the diameter of the loop increases and exhibits a similar shape. This behavior implies the increasing corrosion resistance of the inhibitor and the inhibitor works at the same inhibition mechanism. At lower frequencies, the formation of *WT.E* film is observed in the form of a wide shoulder from the depressed capacitive loop (Fig. 4, *b*). Moreover, the increase of high-frequency phase angle (−60° to −15°) in Bode Phase (Fig. 4, *b*) agreed well with the increased frequency range of Bode Plot impedance (1–4.2 kHz).

This result is mainly demonstrated by the presence of the total phenolic compound in the extract. According to the TPC calculation, the value of TPC in the sample was 14.17±0.25 mg GAE/100 g dried weight. The selection of the solvent is essential to obtain the optimum amount of TPC [46]. In this section, the extraction of White tea was done using acetone 70 % due to solvent polarity. As a result, the solvent penetration within the solid matrix of White tea increases [47] and the amount of the extracted phenol increases accordingly. Smaller concentration of acetone 50 % from the previous study [24] asserts that the TPC value was only about 8 mg GAE/100 g of dried White tea. This result implies that the polar-to-polar interaction, increasing concentration of acetone and temperature of 70 °C, and extending the infusion time for 1 hour, will affect the extractability of phenol from the White tea.

Meanwhile, the effectiveness of inhibition depends on the adsorption stability of the *WT.E* extract. Literature studies show that the value ΔG_{ads} of −20 kJ/mol or less is referred to physisorption, which affirms the van der Waals interaction between the inhibitor and metals [34, 35] whereas; the value beyond −40 kJ/mol or more implies the process of charge sharing and the formation of a dative covalent bond through electronic transfer from the molecule of inhibitor to the surface of metals (chemisorption) [36]. Therefore, the white tea inhibitor appears as chemisorption at high temperatures. Nevertheless, this quantitative value of ΔG_{ads} is insufficient to justify the chemisorption process, but detailed knowledge

of the interaction between the adsorbate (inhibitor) and the adsorbent (the mild steel) is essential to substantiate the chemisorption. In this work, we used Raman spectroscopy as an alternative spectroscopy method to clarify the pertinent functional group adsorbed on the metal surface (Fig. 5, *b*). With this understanding, the spectrum shows the formation of chemisorbed film as a result of the formation of a dative covalent bond (chemical enhancement) between the inhibitor molecule and the Fe ions.

The plotting of ln K_{ads} vs T^{-1} (5) is used to predict the heat of adsorption, ΔH_{ads} and to describe the coverage protection as the function of temperature [37]. The data demonstrate that the adsorption of White tea is partially physisorption and chemisorption, however, the increase in temperature accommodates the chemisorption. It is clear from Table 4, the value of disorder (ΔS_{ads}) indicates that the solid-liquid interface increases upon the adsorption process. The positive value of ΔS_{ads} elicits the thermal stability of the film increases at elevated temperature and their irreversibility process as previously discussed [12]. The reduction of E_a at any concentration and temperature affects the chemisorption process [25]. This fact is comparable to the existing research [39] due to the white tea extract lowers the reaction rate by attached parallelly on the inhibited area.

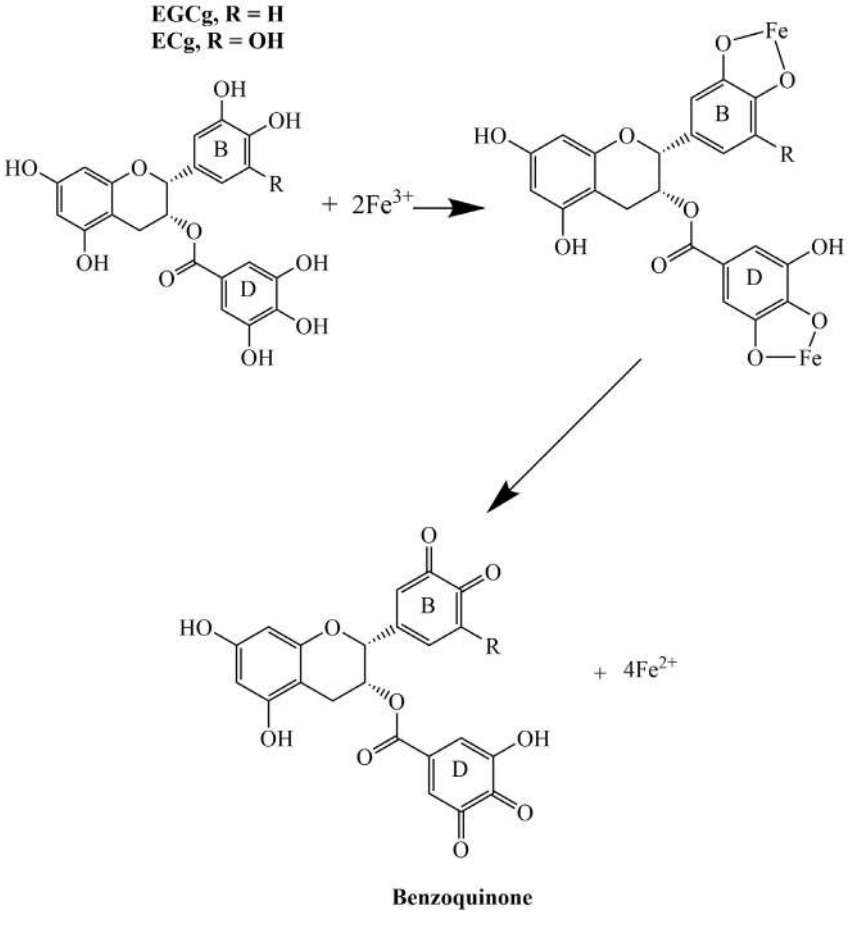

Fig. 9. Proposed inhibition mechanism

Fig. 3, *c* shows the length of the linear region T^{-1} versus ln Corr rate. It correlates to the active sites of inhibitor at 25-60 °C. The slope of the straight line is a key to explaining the number of active sites (Fig. 3, *c*). At 80 ppm solution, the slope was 1.02 greater than 1.0 and it shows that the inhibitor occupies 1.02 active sites on the surface of mild steel as previously mentioned [48]. The greater active sites are consistent with the highest value of inhibition efficiency (96 %) at 60 °C. On the other hand, the contribution of surface coverage of inhibitor, θ, demonstrates that the adsorption increases as a function of temperature. These relativistic effects enhance more active inhibitors to adsorb on the surface of the metal at 60 °C (Fig. 3, *b*).

The limitation on the electrochemical and thermodynamic studies can be addressed by the comprehensive discussion on the spectroscopic results (FTIR and Raman) and the surface analysis (SEM/EDX and AFM). On the one hand, Fig. 6, *a*, shows the presence of -OH in both the spectra of the *WT.E* film and the inhibitor 80 ppm solution is shown at around 3,200 cm^{-1} and 3,295 cm^{-1} as compared to the previous result [49]. This confirms that the hydroxyl is fully deposited on the surface of the film at 60 °C. Moreover, the boarder peak at 3,295 cm^{-1} indicates the chelation reaction between Fe-OH occurs. In contrast, the narrow and peak shifting intensity in inhibited surface spectra illustrates a remarkable reduction capability of inhibitor to reduce the amount of Fe^{3+} ions (in the complex of Fe^{3+}-Inh) (Fig. 9) [38].

A similar result occurs in transition metal ions [50]. Additionally, the medium peak at 2,821 cm^{-1} is attributed to the stretching of the C-H group in the catechin [51]. The disappearance of this peak correlates with an increase in the hydrophobic of the passive film. Twin peaks at 1,638 and 1,697 cm^{-1} show the involvement of the C=O group in White tea as agreed from the previous evidence [52]. This peak shift from 1,697 to 1,638 cm^{-1} is appreciable to describe the deposition of C=O as intermediate (Fig. 4, *a*) [24]. The aryl C=C peak appears in both spectra at 1,423 cm^{-1} [53]. The stretching bands of -CH_3 and C-O functional groups are detected at 1,347 and 1,236. The C-O-C asymmetric [54] and symmetric appears at 1,038 cm^{-1} and 927 cm^{-1}. Hence, the White tea contains -OH, aryl C=C, C=O, and C-O-C symmetric are present both in uninhibited and inhibited systems.

To verify the FTIR results, the Raman spectra present the characteristics of White tea. Fig. 6, *b* presents the comparison between the Raman peaks of the untreated and treated surface of mild steel. The weak peak of -OH appears at 3,003 cm^{-1} and is amplified into higher intensity at 3,102 cm^{-1}, showing that the chosen functional group binds with the Fe atom on the substrate to provide reasonable chemical sorption. The drastic reduction intensity at the peak of 1,563/1,562, 1,478/1,481 and 1,334/1,339 confirms that C=O, Aryl C=C and C-O (vibrational mode) [55] are adsorbed on the surface of the metal. This trend is consistent with the FTIR results. The peak of Fe_2O_3 and in *WT.E* is seen in the range of 300–458 cm^{-1} and 1,061–1,563 cm^{-1},

and well agrees with the earlier research [56]. In the same publication, the author [56] assigns peaks at 300, 532, and 661 cm^{-1} to show the presence of Fe_3O_4. The process of inhibition involves the reduction of $Fe^{3+} \rightarrow Fe^{2+}$. This local mode of analysis shows that the reduction of δ-FeOOH phase appears at 420 and 663 cm^{-1} as agreed previously [57]. Overall, these spectroscopic spectra prove that chemisorbed film and iron corrosion products are retained on the mild steel surface.

On the other hand, the restriction on the surface modification due to the adsorption process can be solved through the comprehensive characterization using SEM/EDX and AFM. The unprotected substrate gives 90.42 % and 6.27 % mass of Fe and Cl. It implies that the precipitation of corrosion products occurred in the form of $Fe(OH)_2$ and $Fe(OH)_3$. The broken mild steel capillarity structure and passive oxide of Fe_2O_3 rise the opportunity of Cl^- to raise the composition of the chlorine [50]. The rise of $[Fe^{2+}]$ in inhibitor solution and formation of Benzoquinone (Mr=108.095 g/mol) are associated with the increment of the oxygen atom. Subsequently, the increasing amount of Fe is the impact of the Fe^{3+} to Fe^{2+} reduction process. Due to low ΔG_{ads} and E_a, the adsorption process at 80 ppm is a feasible process and increases greater surface coverage area of 0.96 with a high K_{ads} value of 0.31. The thickness of the passive film shows the stability of agglomerated particles to reduce the cracks and pitting corrosion. The agglomeration corresponds to the donor-acceptor interaction between the π-electrons of the aromatic and carbonyl molecules to the vacant-3d-orbital of Fe. The excessive negative charge on the surface of metals causes the electron to be transferred to the 3d-orbital. Therefore, the proposed inhibition mechanism is given in (10)–(12) [51],

$$\{Inh \rightleftharpoons Inh^+ + e^-\}, \quad (10)$$

$$\{Inh^+ + Cl^- \rightleftharpoons Inh - Cl(film)\}, \quad (11)$$

$$\{Inh^+ + 2H^+ + 2e^- \rightleftharpoons Inh + H_2\}. \quad (12)$$

Reactions (11) and (12) occur at equilibrium, where the inhibitor acts as an intermediate to inactivate Cl-. Meanwhile, the species of Inh^+ accepts the electron (due to the dissolution of metals) and releases hydrogen gas. However, the limitation of this method gives inadequate access to describe the surface roughness and modification on the atomic level. Hence, we aided this result using the AFM results. Investigation of the surface roughness of the *WT.E* film revealed that the skewness parameter of the film is sufficient to explain the surface modification of the inhibitor. The skewness parameter describes the ratio between the number of peaks and the number of valleys. The negative sign of the skewness corresponds to a larger fraction valley compared to the peak. A sizeable magnitude of the skewness shows more peaks compared to valleys. These values are evidence that the adsorbent has modified the surface of the mild steel and are accountable to reduce the roughness of the uninhibited metals. Qualitatively, the presence of inhibitors covers the pits corrosion through adsorption of the catechin molecules on the surface and increases the effectiveness of the inhibitor.

The presented results serve as alternative development to manufacture White tea as a green corrosion inhibitor. One development that has been accomplished by this research is by maintaining R_{inh} at 59 Ω cm^2 and 60 °C. It gives the ideal cost/benefit of protection at 26.63 mmol/cm^2 due to the formation of stable and thicker adsorbed film. Economically, the volume ratio of the inhibitor over the exposed surface area is at 230 ml/cm^2 at 80 ppm (Fig. 2, *c*). Another consideration is demonstrated based on the proposed inhibition mechanism (Fig. 9). This fact is due to the presence of ligand's peaks, which are intensively seen in the FTIR results (Fig. 6, *a*). Also, both molecules equally participated in the *Fe-Inh* complexing reaction and their local structure is similar. The adjoining triple hydroxyl groups in EGCg act as metal chelators, which bind to two electrophiles of Fe^{3+} ions and reduce an oxidant electronic transfer [58]. The adsorption occurs primarily at the Gallate B and D ring and gives a wider active site and geometric blocking mechanism through chelation (Fig. 9) [59]. Four electrons are dismissed upon decomposition of Fe^{3+}-ECg and Fe^{3+}-EGCg bonding from one mole of ligands [24] to give benzoquinone and Fe^{2+}. As a result, the E_{corr} and i_{corr} values shift to the negative direction while increasing %η. Therefore, white tea extract can be considered a potential prospective green corrosion inhibitor.

The results of this work retain certain limitations. For instance, the utilization of the spectroscopic and surface analysis is unable to confirm the prediction bonding between Fe^{3+}-ECg and Fe^{3+}-EGCg. One source of this weakness is the lack of information to provide the molecular mass of the adsorbed passive film on the surface of the metal. Further work to clarify the presence of ECg and EGCg as two active molecules in White tea is required. These predicted molecules are responsible for the electron donation from the inhibitor molecules to the 3-d orbital of iron. Further studies using HPLC, Mass Spectroscopy, and/or NMR Spectroscopy techniques are needed to validate whether the complexes are fully adsorbed on the surface of metals.

An additional uncontrolled factor is the possibility of the other derivate molecules in White tea such as tannin, which may contribute to increasing the thermal stability of the inhibitor at an elevated temperature of 60 °C. Although the current study is based on the contribution of catechin molecules in the inhibition process, the findings suggest that the orientation of the molecules in White tea on the surface of the metal is also important. Based on the results of [10], the parallel orientation of inhibitor at the Fe (110) plane shows an improvement in the surface coverage and contact of inhibition due to its lowest surface energy. Therefore, future research needs to examine the links between the orientation of the inhibitor molecule and inhibition efficiency.

7. Conclusions

1. The study contributes to our understanding that the phenolic compounds in White tea can be used as a green corrosion inhibitor and reduces the corrosion rate by nearly 85 %.

2. The results of this investigation show that the total phenolic content (TPC) in White tea is approximately 15 % and the findings of this study suggest that the phenol contributes to the adsorption process on mild steel.

3. Prior to this study it was difficult to make predictions about the types of functional groups attached on the mild steel. The combination of FTIR and Raman Spectroscopy findings provides some support for the conceptual premise that -OH, C=O, Aryl C=C, C-O-C are successfully adsorbed on the metal.

4. The thermodynamics calculation confirms that the White tea inhibitor is chemisorption type of inhibitor and adheres to Langmuir isotherm adsorption mode.

5. The most obvious finding to emerge from this study is the surface modification on the metal based on the SEM result. EDX calculation shows the percentage composition of oxygen atom appears to increase while iron and chlorine decrease. AFM results confirm that the impact of adsorption correlates to the reduction of surface roughness.

Acknowledgments

The authors would like to express their gratitude to the Ministry of Research and Technology/National Research and Innovation Agency for the financial support of PDUPT with contract number of NKB-248/UN2.RST/HKP.05.00/2020.

References

1. Atta, N. F., Fekry, A. M., Hassaneen, H. M. (2011). Corrosion inhibition, hydrogen evolution and antibacterial properties of newly synthesized organic inhibitors on 316L stainless steel alloy in acid medium. International Journal of Hydrogen Energy, 36 (11), 6462–6471. doi: https://doi.org/10.1016/j.ijhydene.2011.02.134
2. Pradipta, I., Kong, D., Tan, J. B. L. (2019). Natural organic antioxidants from green tea inhibit corrosion of steel reinforcing bars embedded in mortar. Construction and Building Materials, 227, 117058. doi: https://doi.org/10.1016/j.conbuildmat.2019.117058
3. Goyal, M., Kumar, S., Bahadur, I., Verma, C., Ebenso, E. E. (2018). Organic corrosion inhibitors for industrial cleaning of ferrous and non-ferrous metals in acidic solutions: A review. Journal of Molecular Liquids, 256, 565–573. doi: https://doi.org/10.1016/j.molliq.2018.02.045
4. Ashassi-Sorkhabi, H., Seifzadeh, D., Hosseini, M. G. (2008). EN, EIS and polarization studies to evaluate the inhibition effect of 3H-phenothiazin-3-one, 7-dimethylamin on mild steel corrosion in 1M HCl solution. Corrosion Science, 50 (12), 3363–3370. doi: https://doi.org/10.1016/j.corsci.2008.09.022
5. Kusumastuti, R., Pramana, R. I., Soedarsono, J. W. (2017). The use of morinda citrifolia as a green corrosion inhibitor for low carbon steel in 3.5% NaCl solution. AIP Conference Proceedings. doi: https://doi.org/10.1063/1.4978085
6. Pramana, R. I., Kusumastuti, R., Soedarsono, J. W., Rustandi, A. (2013). Corrosion Inhibition of Low Carbon Steel by Pluchea Indica Less. in 3.5% NaCL Solution. Advanced Materials Research, 785-786, 20–24. doi: https://doi.org/10.4028/www.scientific.net/amr.785-786.20
7. Subekti, N., Soedarsono, J. W., Riastuti, R., Sianipar, F. D. (2020). Development of environmental friendly corrosion inhibitor from the extract of areca flower for mild steel in acidic media. Eastern-European Journal of Enterprise Technologies, 2 (6 (104)), 34–45. doi: https://doi.org/10.15587/1729-4061.2020.197875
8. Ayende, Rustandi, A., Soedarsono, J. W., Priadi, D., Sulistijono, Suprapta, D. N. et. al. (2014). Interaction of Purple Sweet Potato Extract with Ascorbic Acid in $FeCl_3$ Solution. Applied Mechanics and Materials, 680, 32–37. doi: https://doi.org/10.4028/www.scientific.net/amm.680.32
9. Ayende, Rustandi, A., Soedarsono, J. W., Priadi, D., Sulistijono, Suprapta, D. N. et. al. (2014). Effects of Purple Sweet Potato Extract Addition in Ascorbic Acid Inhibitor to Corrosion Rate of API 5L Steel in 3.5 % NaCl Environment. Applied Mechanics and Materials, 709, 384–389. doi: https://doi.org/10.4028/www.scientific.net/amm.709.384
10. Guo, L., Obot, I. B., Zheng, X., Shen, X., Qiang, Y., Kaya, S., Kaya, C. (2017). Theoretical insight into an empirical rule about organic corrosion inhibitors containing nitrogen, oxygen, and sulfur atoms. Applied Surface Science, 406, 301–306. doi: https://doi.org/10.1016/j.apsusc.2017.02.134
11. Lgaz, H., Salghi, R., Jodeh, S., Hammouti, B. (2017). Effect of clozapine on inhibition of mild steel corrosion in 1.0 M HCl medium. Journal of Molecular Liquids, 225, 271–280. doi: https://doi.org/10.1016/j.molliq.2016.11.039
12. Lashgari, S. M., Yari, H., Mahdavian, M., Ramezanzadeh, B., Bahlakeh, G., Ramezanzadeh, M. (2020). Unique 2-methylimidazole based Inorganic Building Brick nano-particles (NPs) functionalized with 3-aminopropyltriethoxysilane with excellent controlled corrosion inhibitors delivery performance; Experimental coupled with molecular/DFT-D simulations. Journal of the Taiwan Institute of Chemical Engineers, 117, 209–222. doi: https://doi.org/10.1016/j.jtice.2020.11.035
13. Røge, R., Møller, B. K., Andersen, C. R., Correll, C. U., Nielsen, J. (2012). Immunomodulatory effects of clozapine and their clinical implications: What have we learned so far? Schizophrenia Research, 140 (1-3), 204–213. doi: https://doi.org/10.1016/j.schres.2012.06.020
14. 2-methylimidazole named as a hazardous chemical (2020). Focus on Catalysts, 2020 (11), 3. doi: https://doi.org/10.1016/j.focat.2020.10.011
15. Caldona, E. B., Zhang, M., Liang, G., Hollis, T. K., Webster, C. E., Smith, D. W., Wipf, D. O. (2021). Corrosion inhibition of mild steel in acidic medium by simple azole-based aromatic compounds. Journal of Electroanalytical Chemistry, 880, 114858. doi: https://doi.org/10.1016/j.jelechem.2020.114858
16. Soedarsono, J. W., Shihab, M. N., Azmi, M. F., Maksum, A. (2018). Study of curcuma xanthorrhiza extract as green inhibitor for API 5L X42 steel in 1M HCl solution. IOP Conference Series: Earth and Environmental Science, 105, 012060. doi: https://doi.org/10.1088/1755-1315/105/1/012060
17. Kaban, E. E., Maksum, A., Permana, S., Soedarsono, J. W. (2018). Utilization of secang heartwood (caesalpinia sappan l) as a green corrosion inhibitor on carbon steel (API 5L Gr. B) in 3.5% NaCl environment. IOP Conference Series: Earth and Environmental Science, 105, 012062. doi: https://doi.org/10.1088/1755-1315/105/1/012062

18. Arlan, A. S., Subekti, N., Soedarsono, J. W., Rustandi, A. (2018). Corrosion Inhibition by a Caesalpinia Sappan L Modified Imidazoline for Carbon Steel API 5L Grade X60 in HCl 1M Environment. Materials Science Forum, 929, 158–170. doi: https://doi.org/10.4028/www.scientific.net/msf.929.158
19. Ayende, Rachmanda, F., Soedarsono, J. W., Priadi, D., Sulistijono, S. (2013). Corrosion Behavior of API-5L in Various Green Inhibitors. Advanced Materials Research, 634-638, 689–695. doi: https://doi.org/10.4028/www.scientific.net/amr.634-638.689
20. Rustandi, A., Soedarsono, J. W., Suharno, B. (2011). The Use of Mixture of Piper Betle and Green Tea as a Green Corrosion Inhibitor for API X-52 Steel in Aerated 3.5 % NaCl Solution at Various Rotation Rates. Advanced Materials Research, 383-390, 5418–5425. doi: https://doi.org/10.4028/www.scientific.net/amr.383-390.5418
21. Verma, C., Verma, D. K., Ebenso, E. E., Quraishi, M. A. (2018). Sulfur and phosphorus heteroatom-containing compounds as corrosion inhibitors: An overview. Heteroatom Chemistry, 29 (4), e21437. doi: https://doi.org/10.1002/hc.21437
22. Loto, R. T. (2018). Surface coverage and corrosion inhibition effect of Rosmarinus officinalis and zinc oxide on the electrochemical performance of low carbon steel in dilute acid solutions. Results in Physics, 8, 172–179. doi: https://doi.org/10.1016/j.rinp.2017.12.003
23. Oliveira, P. F., Tomás, G. D., Dias, T. R., Martins, A. D., Rato, L., Alves, M. G., Silva, B. M. (2015). White tea consumption restores sperm quality in prediabetic rats preventing testicular oxidative damage. Reproductive BioMedicine Online, 31 (4), 544–556. doi: https://doi.org/10.1016/j.rbmo.2015.06.021
24. Ryan, P., Hynes, M. J. (2007). The kinetics and mechanisms of the complex formation and antioxidant behaviour of the polyphenols EGCg and ECG with iron(III). Journal of Inorganic Biochemistry, 101 (4), 585–593. doi: https://doi.org/10.1016/j.jinorgbio.2006.12.001
25. Pradipta, I., Kong, D., Tan, J. B. L. (2019). Natural organic antioxidants from green tea form a protective layer to inhibit corrosion of steel reinforcing bars embedded in mortar. Construction and Building Materials, 221, 351–362. doi: https://doi.org/10.1016/j.conbuildmat.2019.06.006
26. Yadav, M., Sinha, R. R., Kumar, S., Sarkar, T. K. (2015). Corrosion inhibition effect of spiropyrimidinethiones on mild steel in 15% HCl solution: insight from electrochemical and quantum studies. RSC Advances, 5 (87), 70832–70848. doi: https://doi.org/10.1039/c5ra14406j
27. Verma, C., Olasunkanmi, L. O., Ebenso, E. E., Quraishi, M. A. (2018). Substituents effect on corrosion inhibition performance of organic compounds in aggressive ionic solutions: A review. Journal of Molecular Liquids, 251, 100–118. doi: https://doi.org/10.1016/j.molliq.2017.12.055
28. El-Abbasy, H. M., Nazeer, A. A., Fouda, A. S. (2016). Electrochemical assessment of inhibitive behavior of some antibacterial drugs on 316 stainless steel in acidic medium. Protection of Metals and Physical Chemistry of Surfaces, 52 (3), 562–573. doi: https://doi.org/10.1134/s2070205116030084
29. Shabri, S., Rohdiana, D. (2016). Optimization and characterization of green tea polyphenol extract from various solvents. Jurnal Penelitian Teh Dan Kina, 19 (1). doi: https://doi.org/10.22302/pptk.jur.jptk.v19i1.82
30. Ebenso, E. E., Eddy, N. O., Odiongenyi, A. O. (2008). Corrosion inhibitive properties and adsorption behaviour of ethanol extract of Piper guinensis as a green corrosion inhibitor for mild steel in H2SO4. African Journal of Pure and Applied Chemistry, 2 (11), 107–115. Available at: https://www.researchgate.net/publication/285020680_Corrosion_inhibitive_properties_and_adsorption_behaviour_of_ethanol_extract_of_Piper_guinensis_as_a_green_corrosion_inhibitor_for_mild_steel_in_H_2SO_4
31. Singleton, V. L., Orthofer, R., Lamuela-Raventós, R. M. (1999). Analysis of total phenols and other oxidation substrates and antioxidants by means of folin-ciocalteu reagent. Methods in Enzymology, 152–178. doi: https://doi.org/10.1016/s0076-6879(99)99017-1
32. Calderón, J. A., Vásquez, F. A., Carreño, J. A. (2017). Adsorption and performance of the 2-mercaptobenzimidazole as a carbon steel corrosion inhibitor in EDTA solutions. Materials Chemistry and Physics, 185, 218–226. doi: https://doi.org/10.1016/j.matchemphys.2016.10.026
33. Ghailane, T., Balkhmima, R. A., Ghailane, R., Souizi, A., Touir, R., Ebn Touhami, M. et. al. (2013). Experimental and theoretical studies for mild steel corrosion inhibition in 1M HCl by two new benzothiazine derivatives. Corrosion Science, 76, 317–324. doi: https://doi.org/10.1016/j.corsci.2013.06.052
34. Chelliah, N. M., Padaikathan, P., Kumar, R. (2019). Evaluation of electrochemical impedance and biocorrosion characteristics of as-cast and T4 heat treated AZ91 Mg-alloys in Ringer's solution. Journal of Magnesium and Alloys, 7 (1), 134–143. doi: https://doi.org/10.1016/j.jma.2019.01.005
35. Siddiqui, N., Rauf, A., Latif, A., Mahmood, Z. (2017). Spectrophotometric determination of the total phenolic content, spectral and fluorescence study of the herbal Unani drug Gul-e-Zoofa (Nepeta bracteata Benth). Journal of Taibah University Medical Sciences, 12 (4), 360–363. doi: https://doi.org/10.1016/j.jtumed.2016.11.006
36. Piluzza, G., Bullitta, S. (2011). Correlations between phenolic content and antioxidant properties in twenty-four plant species of traditional ethnoveterinary use in the Mediterranean area. Pharmaceutical Biology, 49 (3), 240–247. doi: https://doi.org/10.3109/13880209.2010.501083
37. Sedik, A., Lerari, D., Salci, A., Athmani, S., Bachari, K., Gecibesler, İ. H., Solmaz, R. (2020). Dardagan Fruit extract as eco-friendly corrosion inhibitor for mild steel in 1 M HCl: Electrochemical and surface morphological studies. Journal of the Taiwan Institute of Chemical Engineers, 107, 189–200. doi: https://doi.org/10.1016/j.jtice.2019.12.006

38. Li, X.-H., Deng, S.-D., Fu, H. (2010). Inhibition by Jasminum nudiflorum Lindl. leaves extract of the corrosion of cold rolled steel in hydrochloric acid solution. Journal of Applied Electrochemistry, 40 (9), 1641–1649. doi: https://doi.org/10.1007/s10800-010-0151-5
39. Sanni, O., Popoola, A. P. I., Fayomi, O. S. I. (2019). Temperature Effect, Activation Energies and Adsorption Studies of Waste Material as Stainless Steel Corrosion Inhibitor in Sulphuric Acid 0.5 M. Journal of Bio- and Tribo-Corrosion, 5 (4). doi: https://doi.org/10.1007/s40735-019-0280-2
40. Singh, A. K., Quraishi, M. A. (2011). Investigation of the effect of disulfiram on corrosion of mild steel in hydrochloric acid solution. Corrosion Science, 53 (4), 1288–1297. doi: https://doi.org/10.1016/j.corsci.2011.01.002
41. Bentiss, F., Lebrini, M., Lagrenée, M. (2005). Thermodynamic characterization of metal dissolution and inhibitor adsorption processes in mild steel/2,5-bis(n-thienyl)-1,3,4-thiadiazoles/hydrochloric acid system. Corrosion Science, 47 (12), 2915–2931. doi: https://doi.org/10.1016/j.corsci.2005.05.034
42. Khodyrev, Y. P., Batyeva, E. S., Badeeva, E. K., Platova, E. V., Tiwari, L., Sinyashin, O. G. (2011). The inhibition action of ammonium salts of O,O′-dialkyldithiophosphoric acid on carbon dioxide corrosion of mild steel. Corrosion Science, 53 (3), 976–983. doi: https://doi.org/10.1016/j.corsci.2010.11.030
43. Scardino, A. J., Hudleston, D., Peng, Z., Paul, N. A., de Nys, R. (2009). Biomimetic characterisation of key surface parameters for the development of fouling resistant materials. Biofouling, 25 (1), 83–93. doi: https://doi.org/10.1080/08927010802538480
44. Noorbakhsh Nezhad, A. H., Davoodi, A., Mohammadi Zahrani, E., Arefinia, R. (2020). The effects of an inorganic corrosion inhibitor on the electrochemical behavior of superhydrophobic micro-nano structured Ni films in 3.5% NaCl solution. Surface and Coatings Technology, 395, 125946. doi: https://doi.org/10.1016/j.surfcoat.2020.125946
45. King, A. D., Birbilis, N., Scully, J. R. (2014). Accurate Electrochemical Measurement of Magnesium Corrosion Rates; a Combined Impedance, Mass-Loss and Hydrogen Collection Study. Electrochimica Acta, 121, 394–406. doi: https://doi.org/10.1016/j.electacta.2013.12.124
46. Sultana, B., Anwar, F., Ashraf, M. (2009). Effect of Extraction Solvent/Technique on the Antioxidant Activity of Selected Medicinal Plant Extracts. Molecules, 14 (6), 2167–2180. doi: https://doi.org/10.3390/molecules14062167
47. Bhebhe, M., Füller, T. N., Chipurura, B., Muchuweti, M. (2015). Effect of Solvent Type on Total Phenolic Content and Free Radical Scavenging Activity of Black Tea and Herbal Infusions. Food Analytical Methods, 9 (4), 1060–1067. doi: https://doi.org/10.1007/s12161-015-0270-z
48. Villamil, R. F. V., Corio, P., Agostinho, S. M. L., Rubim, J. C. (1999). Effect of sodium dodecylsulfate on copper corrosion in sulfuric acid media in the absence and presence of benzotriazole. Journal of Electroanalytical Chemistry, 472 (2), 112–119. doi: https://doi.org/10.1016/s0022-0728(99)00267-3
49. Porcayo-Calderon, J., Martínez De La Escalera, L. M., Canto, J., Casales-Diaz, M. (2015). Imidazoline derivatives based on coffee oil as CO_2 corrosion inhibitor. International Journal of Electrochemical Science, 10 (3), 3160–3176. Available at: https://www.researchgate.net/publication/272942244_Imidazoline_Derivatives_Based_on_Coffee_Oil_as_CO2_Corrosion_Inhibitor
50. Azizi, S., Mahdavi Shahri, M., Rahman, H., Abdul Rahim, R., Rasedee, A., Mohamad, R. (2017). Green synthesis palladium nanoparticles mediated by white tea (Camellia sinensis) extract with antioxidant, antibacterial, and antiproliferative activities toward the human leukemia (MOLT-4) cell line. International Journal of Nanomedicine, 12, 8841–8853. doi: https://doi.org/10.2147/ijn.s149371
51. Li, X.-H., Deng, S.-D., Fu, H., Mu, G.-N. (2009). Inhibition by tween-85 of the corrosion of cold rolled steel in 1.0 M hydrochloric acid solution. Journal of Applied Electrochemistry, 39 (7), 1125–1135. doi: https://doi.org/10.1007/s10800-008-9770-5
52. Bahrami, M. J., Hosseini, S. M. A., Pilvar, P. (2010). Experimental and theoretical investigation of organic compounds as inhibitors for mild steel corrosion in sulfuric acid medium. Corrosion Science, 52 (9), 2793–2803. doi: https://doi.org/10.1016/j.corsci.2010.04.024
53. Tarantilis, P. A., Troianou, V. E., Pappas, C. S., Kotseridis, Y. S., Polissiou, M. G. (2008). Differentiation of Greek red wines on the basis of grape variety using attenuated total reflectance Fourier transform infrared spectroscopy. Food Chemistry, 111 (1), 192–196. doi: https://doi.org/10.1016/j.foodchem.2008.03.020
54. Li, X. H., Deng, S. D., Fu, H., Mu, G. N. (2009). Inhibition action of tween-80 on the corrosion of cold rolled steel in sulfuric acid. Materials and Corrosion, 60 (12), 969–976. doi: https://doi.org/10.1002/maco.200905217
55. Jurasekova, Z., Domingo, C., Garcia-Ramos, J. V., Sanchez-Cortes, S. (2014). Effect of pH on the chemical modification of quercetin and structurally related flavonoids characterized by optical (UV-visible and Raman) spectroscopy. Physical Chemistry Chemical Physics, 16 (25), 12802–12811. doi: https://doi.org/10.1039/c4cp00864b
56. Hanesch, M. (2009). Raman spectroscopy of iron oxides and (oxy)hydroxides at low laser power and possible applications in environmental magnetic studies. Geophysical Journal International, 177 (3), 941–948. doi: https://doi.org/10.1111/j.1365-246x.2009.04122.x
57. Soler, M. A. G., Qu, F. (2012). Raman Spectroscopy of Iron Oxide Nanoparticles. Raman Spectroscopy for Nanomaterials Characterization, 379–416. doi: https://doi.org/10.1007/978-3-642-20620-7_14
58. Zhong, Y., Ma, C.-M., Shahidi, F. (2012). Antioxidant and antiviral activities of lipophilic epigallocatechin gallate (EGCG) derivatives. Journal of Functional Foods, 4 (1), 87–93. doi: https://doi.org/10.1016/j.jff.2011.08.003
59. Cen, H., Chen, Z., Guo, X. (2019). N, S co-doped carbon dots as effective corrosion inhibitor for carbon steel in CO_2-saturated 3.5% NaCl solution. Journal of the Taiwan Institute of Chemical Engineers, 99, 224–238. doi: https://doi.org/10.1016/j.jtice.2019.02.036